Langmuir

Article

pubs.acs.org/Langmuir

Molecular Dynamics Simulations of Liquid Phase Interfaces: Understanding the Structure of the Glycerol/Water−Dodecane System

Frank R. Beierlein,[†,‡] Andreas M. Krause,[†,‡] Christof M. Jäger,[†,‡] Piotr Fita,[§,∥] Eric Vauthey,[§] and Timothy Clark*[,†,‡]

[†]Computer-Chemie-Centrum and Interdisciplinary Center for Molecular Materials, Friedrich-Alexander-Universität Erlangen-Nürnberg, Nägelsbachstr. 25, 91052 Erlangen, Germany

[‡]Excellence Cluster Engineering of Advanced Materials, Friedrich-Alexander-Universität Erlangen-Nürnberg, Nägelsbachstr. 49b, 91052 Erlangen, Germany

[§]Department of Physical Chemistry, University of Geneva, 30 quai Ernest-Ansermet, CH-1211 Geneva 4, Switzerland

[∥]Institute of Experimental Physics, Faculty of Physics, University of Warsaw, ul. Hoza 69, 00-681 Warsaw, Poland

Supporting Information

ABSTRACT: Modern spectroscopic techniques such as time-resolved second-harmonic-generation spectroscopy allow molecules to be examined selectively directly at phase interfaces. Two-phase systems formed by glycerol/water and alkane layers have previously been studied by time-resolved second-harmonic-generation spectroscopic measurements. In this molecular dynamics study, a triphenylmethane dye was inserted at the glycerol/water−alkane interface and was used as a probe for local properties such as viscosity. We now show how extensive simulations over a wide range of concentrations can be used to obtain a detailed view of the molecular structure at the glycerol/water−alkane interface. Glycerol is accumulated in a double layer adjacent to the alkane interface, which results in increased viscosity of the glycerol/water phase in the direct vicinity of the interface. We also show that conformational ensembles created by classical molecular-dynamics simulations can serve as input for QM/MM calculations, yielding further information such as transition dipoles, which can be compared with spectroscopic measurements.

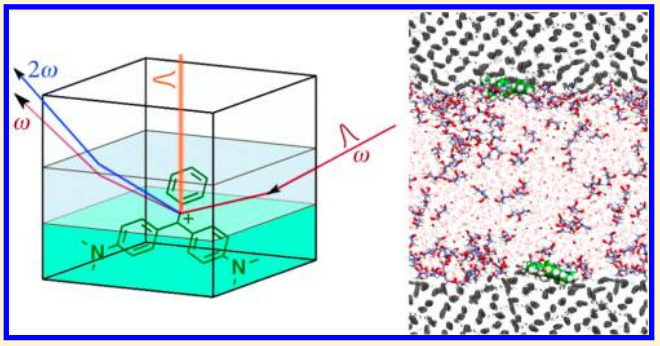

INTRODUCTION

Interfaces, at which different phases are in close contact, are of special interest because the properties of the molecules at the interface can differ decidedly from those in the bulk. Due to the asymmetry of the forces, molecules at interfaces are frequently observed to be more ordered than in the bulk, where more random orientations are usually observed.[1,2] As a result, even such fundamental characteristics as pH and equilibrium constants can differ dramatically.[3,4]

While it is difficult to probe interfaces with linear optical spectroscopy because of the preponderance of molecules in the bulk, nonlinear optical techniques such as second harmonic generation (SHG), sum frequency generation (SFG), or difference frequency generation (DFG) have been used increasingly to study interfaces in recent years,[5−23] as they allow interface species to be probed selectively. In addition to the steady-state forms of these techniques, time-resolved variations have been developed.[5,12,16,23−25] For example, time-resolved second harmonic generation (TRSHG) or time-resolved electronic sum frequency generation (TR-ESFG) can be used to measure the excited-state deactivation of a dye molecule at an interface. The dye acts as a probe, and can be used to determine a property of interest, e.g. local viscosity, directly at the interface.[12,23]

In nonlinear optical techniques like SHG and related techniques, high field strengths are used, and the polarization of the medium is therefore no longer proportional to the incoming field, that is, higher-order terms in the polarization expansion can no longer be neglected. In SHG, SFG, and DFG, a second-order polarization and an associated nonzero second-order nonlinear susceptibility $\chi^{(2)}$ are observed and therefore, in addition to the linear response, light of twice the incident frequency (SHG), the sum frequency (SFG), or the difference frequency (DFG) is generated.[7] Liquids, gases, centrosymmetric materials and all materials with an inversion center have a zero second order susceptibility, in contrast to molecules

Received: June 5, 2013
Revised: August 14, 2013
Published: August 27, 2013

located at interfaces, where symmetry breaking leads to a nonvanishing $\chi^{(2)}$. Hence, interface molecules can be studied selectively by second-order techniques like SHG.[7] Frequently, a dye with a large second-order polarizability, like malachite green (MG), is added to the system of interest, and is used as a probe or indicator molecule.[12,23,26,27]

Glycerol−water solutions have been investigated intensively in recent years,[12,28−31] not only out of theoretical interest, but also because they are widely used in the pharmaceutical and cosmetic industries and as cryoprotective agents. Also, glycerol−water mixtures offer an easy way to fine-tune the viscosity of a polar (water) phase, for example, in spectroscopic studies.[12,32,33] The bulk behavior of glycerol−water mixtures and the behavior of water/glycerol at interfaces have been studied experimentally.[12,28] However, details of the molecular structure at the interface remain scarce, leaving room for much speculation.

To investigate the interface formed by a water/glycerol phase and an alkane, Fita, Punzi, and Vauthey (FPV) performed transient absorption and TRSHG spectroscopic measurements in which they investigated a series of glycerol/water mixtures with different concentrations of glycerol, both in the bulk and at the interface with alkanes.[12] To enhance SHG, they added two different triphenylmethane dyes (malachite green, MG, and brilliant green, BG, Chart 1) to the water/glycerol mixtures.

Chart 1. Structures of Malachite Green (MG, a) and Brilliant Green (BG, b)

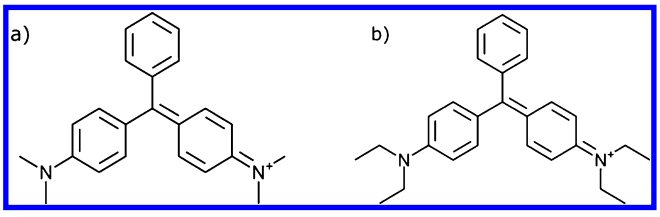

The dyes adsorb at the interface formed with the alkane and are the origin of the resonantly enhanced SHG signal. They are also of special interest themselves as there is controversy about their exact excited-state deactivation mechanisms. In particular, it is unclear if all three rings are required to rotate in the initial step of the radiationless deactivation of the first excited singlet states of MG and BG,[12,32] or if only a rotation of the two aniline rings[5,6] takes place in the barrierless formation of the intermediate, which then returns to the electronic ground state in a radiationless decay process. The notion that the individual rings protrude into different phases (and hence their rotation may possibly be influenced by tuning the viscosity of these phases) has been the basis of several studies that have tried to clarify the deactivation mechanism of triphenylmethane dyes.[5,12] Two of three lifetime components of the excited state are found to depend strongly on the viscosity of the medium (eq 1; τ, lifetime; η, viscosity; α, fitting parameter), as friction is exerted on the rotating rings by the environment. FPV used TRSHG to measure the decay times of the excited states of the dyes MG and BG, both in order to use the dyes as probes for local viscosity and to investigate the exact deactivation mechanism of the dyes.[12]

$$\tau(\eta) \sim \eta^{\alpha} \quad (1)$$

FPV also showed that the decay times obtained with either dye (MG or BG) in various water/glycerol mixtures at the water/dodecane interface are almost four times larger than the shortest viscosity-dependent decay time measured in bulk aqueous solutions. This slow-down was attributed to the increase of the friction exerted by interfacial water on the dye at the interface compared to the situation in the bulk because the decay time of MG at a water/alkane interface was found to be relatively independent of the viscosity of the alkane phase. FPV interpret these results as an indication that there is a structural modification of water several molecular layers below the interface and that the layer of water that exhibits a higher viscosity encompasses the aniline groups of either dye completely, including the alkyl substituents.[12]

FPV also observed that the relaxation of the excited dyes is less affected by the addition of glycerol at interfaces than in bulk solutions, which suggests that the local structure of the liquids plays a major role in the increase of the frictional resistance in the interfacial layer, and that the addition of glycerol contributes only to a lesser extent. They could not exclude that the number of glycerol molecules is reduced close to the interface compared to the bulk liquid (because of a reduced solubility of glycerol in the interfacial layer).[12]

In a complementary study to that by FPV, Tahara and co-workers used TR-ESFG to MG at the air/water interface to investigate the local interface viscosity.[23] They found that the ground-state recovery of MG at the air/water interface is much slower than that in bulk water and almost equivalent to that in a glycerol−water mixture containing glycerol volume fractions as high as 65−80%. They interpret this result as indicating a higher local viscosity at the interface than in bulk water. However, the apparent very large viscosity values evaluated are only valid if other factors (such as changes in the potential energy hypersurface for the dye) are negligible. Thus, the authors emphasize the importance of both changes in the physicochemical properties at the interface and in the dynamics of the indicator molecule (MG) itself.[23]

Earlier work by Eisenthal and co-workers,[5] in which time-resolved measurements were supplemented by analysis of the polarization of the second-harmonic light radiated from the interface (water/air, water/octane, and water/pentadecane interfaces), indicated that the phenyl group of the dye points toward the alkane phase, whereas the aniline substituents are submerged in water and the molecules are tilted by approximately 42° with respect to the interface normal.

In contrast to earlier studies, which assume that the rotation of the phenyl ring (projecting into the alkane phase) is not involved in the deactivation of the excited state of MG,[5,6] FPV conclude that the rotation of all three rings of the dye is involved in the radiationless deactivation; however, because of the smaller molecular volume of the phenyl ring, its rotation rapidly follows the motion of aniline groups when the phenyl ring is surrounded by a low-viscosity medium. The rotation of the phenyl ring becomes a bottleneck for the relaxation only in highly viscous liquids (e.g., paraffin oil instead of shorter alkanes like dodecane in the upper phase), where the effect of the increased viscosity of the upper phase can be seen.[12]

FPV identified three distinct deactivation processes following optical excitation (see Figure 1), the two slower of which were described by the same power function of viscosity, which leads to the conclusion that they can be associated with a twist and twist-back of the aromatic rings attached to the central carbon atom. This is seen as additional evidence supporting the identification of the intermediate state appearing in the

dx.doi.org/10.1021/la4021355 | Langmuir 2013, 29, 11898−11907

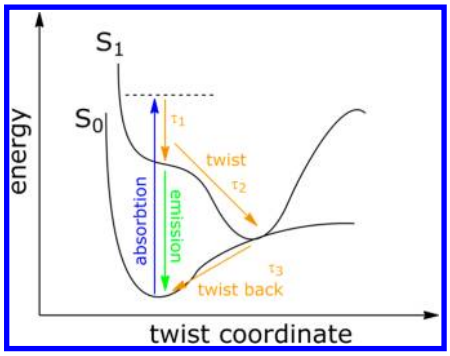

Figure 1. Proposed deactivation mechanism of the excited state of malachite green and brilliant green. (Adapted with permission from ref 12. Copyright 2012 American Chemical Society.)

relaxation pathway of MG and BG as the twisted form of the molecule.[12]

Molecular dynamics (MD) simulations have been used increasingly to understand the structure of soft matter. They are, in some cases, the only tool to understand complex experimental phenomena,[34] and they allow direct insight into molecular structures which are sometimes inaccessible to experiment.[34,35] In order to complement the FPV measurements[12] and to obtain a detailed view of the interface structure, we have performed extensive molecular dynamics simulations of a two-phase system formed by glycerol/water and dodecane, with MG and BG at the interfaces, and over a wide range of glycerol concentrations. The results are described below.

COMPUTATIONAL DETAILS

In the experiment, different mixtures ("sample solution") were obtained by diluting a glycerol "stock-solution" containing 86 mass % glycerol with water,[12] yielding a concentration range from 20.6 to 45.5 vol % glycerol stock-solution in water. For the present work, we converted these concentrations to molar concentrations (0.843−2.04 mol L^{-1}; see Table S5 in the Supporting Information). To cover the experimental concentration range, 33 sets of MD simulations were performed. Simulations were set up using AmberTools 1.2 as included in the Amber 10 Suite.[36] The initial geometries of MG, BG (Chart 1), glycerol, and dodecane were set up in Materials Studio 4.4[37] and subsequently optimized using the semiempirical Hamiltonian AM1[38] with the program Vamp 10.[39] AM1-bcc-charges[40,41] were extracted from the calculations using Antechamber[42] from the Amber suite.

To construct the dodecane phase, dodecane was solvated in itself using Amber 10 Leap.[36] For the glycerol/water phase, a similar procedure was used: glycerol was solvated in itself. Then, TIP3P[43] water molecules were added to the glycerol phase. The different concentrations were obtained by removing individual glycerol molecules. The phases were pasted together and one dye molecule (MG or BG) was placed at each phase interface between the water/glycerol and dodecane phase using a custom-made Perl[44] script. The final system (e.g., for concentration 1.23 mol L^{-1}) consisted of 1 MG molecule, 1 BG molecule, 62 glycerol, 1451 water, and 158 dodecane molecules, and 2 Cl^- ions for charge neutrality (see Table S5 in the Supporting Information for a complete list of concentrations and particle numbers). As a result of the setup procedure, the two interfaces in the system are parallel to the *xy*-plane. General Amber Force Field (gaff) parameters[45] suitable[46,47] for nonprotein simulations were adapted for MG, BG, glycerol, and dodecane. Parameters not included in the standard gaff parameter files are given in Tables S1−S4 in the Supporting Information.

The initial geometry optimization was performed using Amber 10 Sander.[36] One thousand steps of geometry optimization (500 steps steepest decent and 500 steps conjugated gradient) were performed

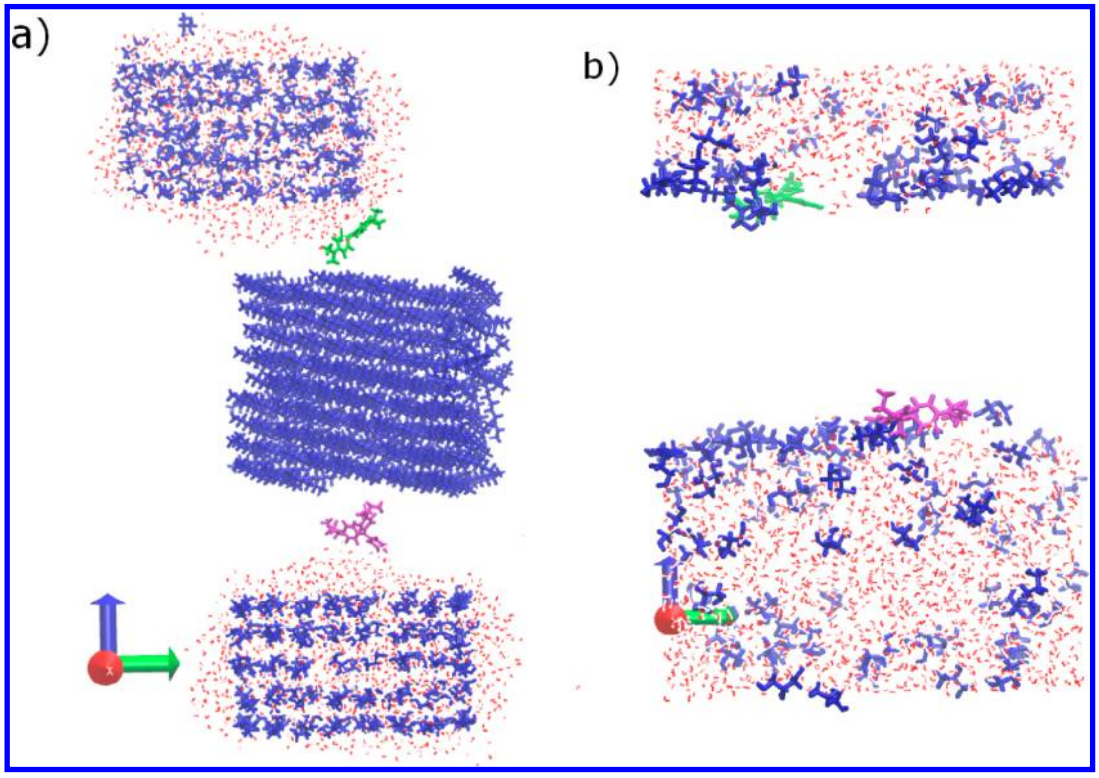

Figure 2. (a) Initial setup of the simulation cell. Blue: glycerol and dodecane molecules. Red: water molecules. Green: malachite green. Magenta: brilliant green. (b) Simulation cell after 46.2 ns (beginning of the analysis interval). Dodecane molecules are omitted for clarity. The data shown correspond to the simulation with 1.23 mol L^{-1} glycerol in water. Figures were created using VMD.[65,66]

dx.doi.org/10.1021/la4021355 | *Langmuir* 2013, 29, 11898−11907

using weak restraints (50 kcal mol^{-1} Å^{-2}) on the heavy atoms of all molecules, followed by 5000 steps of unrestrained minimization. The optimized structures were used as input for Langevin dynamics simulations at 298 K using a 2 fs time step and a collision frequency of 2 ps^{-1}. Bonds involving hydrogen were constrained using SHAKE.[48] The distance cutoff for all nonbonding interactions was set to 10 Å. Long range electrostatics were described by the particle mesh Ewald method.[49,50] For van der Waals interactions beyond those included in the direct sum, a continuum model correction for energy and pressure was used, as implemented in Amber 10. A rectangular box was simulated using periodic boundary conditions. System heat-up was performed during a 200 ps constant volume (NVT) simulation with weak restraints (50 kcal mol^{-1} Å^{-2}). The system was then simulated for 56 ns at constant pressure (NPT) (1 bar, weak pressure coupling, isotropic position scaling, pressure relaxation time 2 ps) without any restraints. Energy and geometry were written out every ps, only the last 10 ns were used for data analysis.

The approximate location of the interfaces was determined by calculating the mean of the *z*-coordinates of the glycerol atom closest to the neighboring dodecane phase and the dodecane atom closest to the glycerol/water phase (see Figure S12 in the Supporting Information for an illustration). Visual inspection of the simulation trajectories showed that the interfaces were not tilted with respect to the *xy*-plane, thus ensuring that the above procedure was sufficient. Distance-distribution functions for the different concentrations (Figure 5) were calculated using the centers of mass of the glycerol molecules plotted vs the distance from the interface defined as above, using a bin size of 1 Å.

QM/MM calculations were performed with VAMP 10.0[39] using the AM1 Hamiltonian.[38] The dye was treated quantum mechanically and the remainder of the system as a rigid point-charge environment.[51] MM charges were taken from the force field, as shown above. The polarization of the QM wave function by the point charges in the MM environment was taken into account *via* an additional one-electron term in the Fock matrix.[51−53] No back-polarization of the MM part by the QM part was included. As explicit solvent molecules were present, we used a constant dielectric constant of 1.0 for both the MM- and the QM/MM-Coulomb interactions. For more details of the QM/MM implementation, see references.[34,51,53−57] The energies and characteristics of the excited states were calculated using configuration interaction that included single and pair double excitations.[58] The transition dipoles corresponding to the $S_0 \rightarrow S_2$ transition (which is approximately resonant with the second harmonic of the 800 nm probe pulse) were extracted from the outputs for a subset of the MD ensemble (100 snapshots, one structure every 100 ps), and visualized using Jmol 9.1[59] and gnuplot.[60] Further details are given in the Supporting Information.

In order to compare the time scales of the movement of the chromophore as obtained from MD (2 fs time step) with the situation perceived by the SHG probe pulses (120 fs fwhm),[12] a part (2000 fs) of the MD simulation was rerun saving snapshots every other fs (1000 snapshots), which also served as a structural basis for QM/MM calculations as explained above.

To validate the quality of the atomistic force field parameters for the use in the simulations of the biphasic systems we have determined densities and self-diffusion coefficients for simulations of bulk glycerol and dodecane and bulk glycerol−water mixtures with different concentrations (see Table S6 in the Supporting Information). The simulations were performed for 10.2 ns each (200 ps NVT heat-up and 10 ns NPT simulation) and show very good agreement with experimental literature values for both bulk properties[61−64] (Table S6 and Figures S10−11 in the Supporting Information).

RESULTS

In the initial setup, the glycerol molecules were distributed evenly over the glycerol−water phase (Figure 2a). At the beginning of the analysis interval (46.2 ns), an accumulation of glycerol molecules near the interface is observed for all concentrations (Figure 2b). The phase interfaces are parallel to the *xy*-plane in all simulation cells. The histograms of the *z*-components of the geometric centers of all molecules ("*z*-plot") show the enrichment of glycerol molecules at the interface more clearly (see, e.g., Figure 3, 1.23 mol L^{-1} glycerol in water).

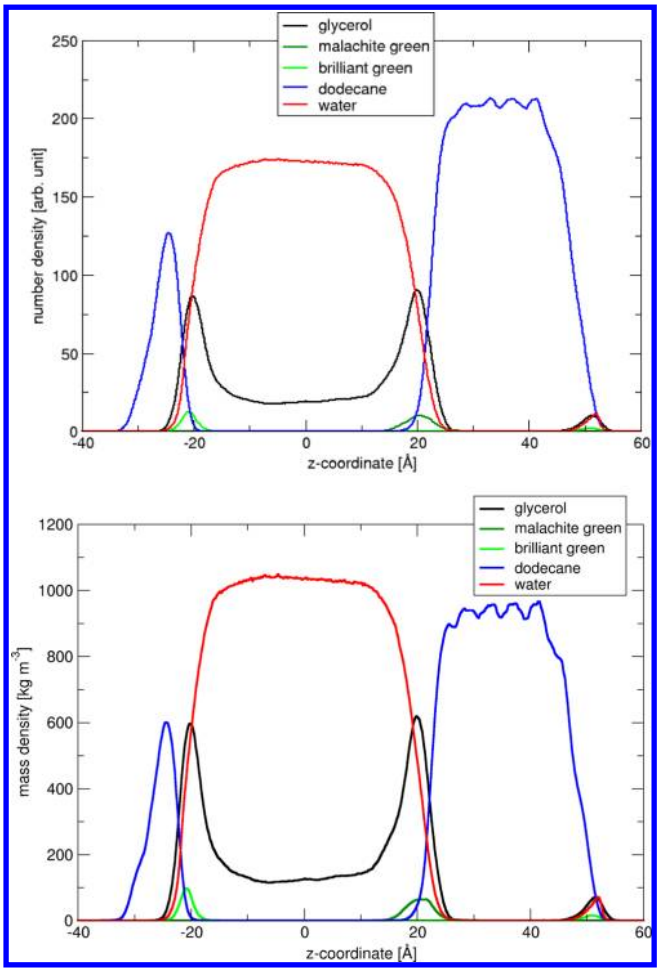

Figure 3. Number density (above) and mass density (below) of glycerol (black), water (red), dodecane (blue), and the dyes malachite green and brilliant green (green, see legend) along the *z*-axis of the simulation cell during the last 10 ns of the simulation (46.2−56.2 ns, bin size 1 Å). The data shown correspond to the simulation with 1.23 mol L^{-1} glycerol in water, and are normalized with respect to the number of molecules and the number of snapshots. The system was centered on the center of mass of all water molecules prior to analysis. Analyses were performed using a modified version of AmberTools ptraj provided by Hannes Loeffler.[67]

The dye molecules (malachite green and brilliant green) are located within an approximately ±5 Å interval from the interfaces over the whole simulation time for all concentrations investigated. An analysis of the relative concentration of glycerol molecules near the interface (glycerol peak height in Figure 3) shows that the relative number of glycerol molecules near the interface decreases at higher concentrations (Figure 4).

For a deeper analysis of the glycerol−water phase structure near the interface, the distance distribution functions of glycerol with respect to the interface were calculated (Figure 5) (distance of the closest atom of each glycerol molecule from the interface plane, bin size 1 Å). The distribution of glycerol within the glycerol−water phase reveals two layers with a higher probability of presence for glycerol molecules (Figure

dx.doi.org/10.1021/la4021355 | *Langmuir* 2013, 29, 11898−11907

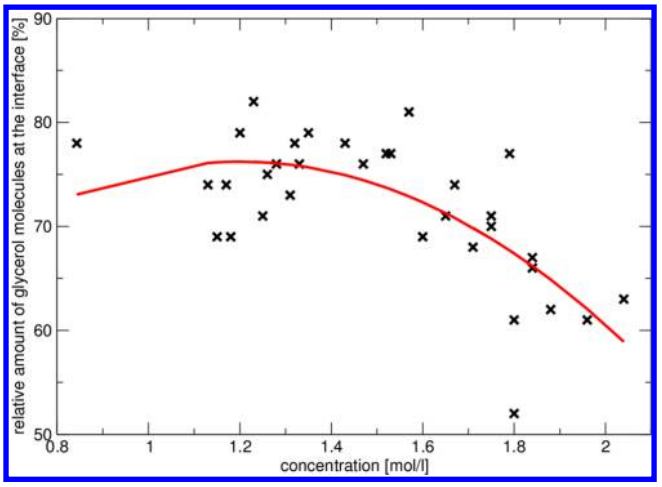

Figure 4. Relative concentration of glycerol molecules within 8 Å from the interface, calculated by dividing the number of glycerol molecules near the interface by the total number of glycerol molecules at a given concentration. The red line is a guide to the eye.

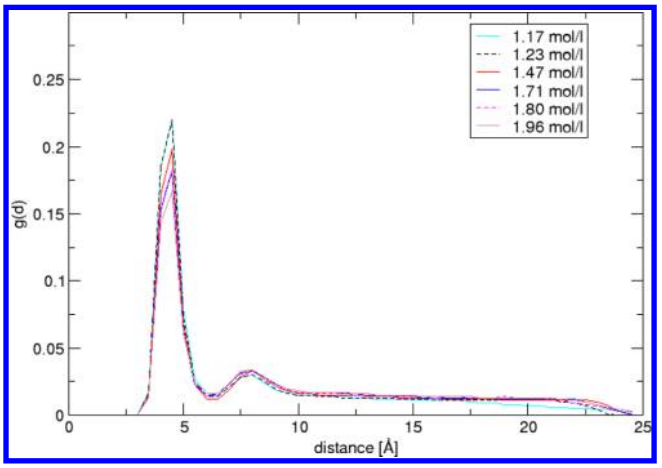

Figure 5. Distribution of the glycerol molecules with respect to the interfaces, normalized by the total number of glycerol molecules and the number of snapshots (interface plane at 0 Å, bin size 1 Å, data symmetrized for both interfaces). Concentrations of glycerol in water (mol L^{-1}) are given in the legend. For clarity, only a subset of the 33 concentrations investigated is shown. At about 25 Å, the distribution function vanishes due to the limited box size.

5). Potentials of mean force were calculated from the distribution functions according to eq 2 (Figure S1 in the Supporting Information),

$$A(r) = -k_B T \ln(g(d)) \quad (2)$$

where A is the Helmholtz free energy, $g(d)$ the distribution function, and T the temperature.

Cross sections of the energy differences between the potentials of mean force for molecules at distances of 4 Å (first minimum/glycerol layer in Figure S1), 6 Å (activation barrier between first and second glycerol layer), and 7.5 Å (second glycerol layer) from the interface are shown in the Supporting Information, Figures S2 and S3. While the energies of the activation barrier at 6 Å and the second glycerol layer at 7.5 Å are almost constant for all concentrations investigated, the energy of the glycerol molecules in the first layer (4 Å) increases moderately with higher concentrations. Therefore, the energy difference between the first layer and the barrier and the difference between the first and the second layer decrease with increasing glycerol concentration (Figures S2 and S3 in the Supporting Information).

In order to analyze the orientation of the dye chromophores relative to the interface, vectors were defined that represent the orientation of the aromatic rings of the triphenyl systems (Chart S3 in the Supporting Information). The mean deviation of these vectors from the interface (*xy*-plane) was calculated and lies within ±20° for all concentrations investigated (Figure S4 in the Supporting Information).

Figure 6 shows the normalized average mean square displacements of the glycerol molecules for the different concentrations. The average mean square displacement of the glycerol molecules was calculated and divided by the number of

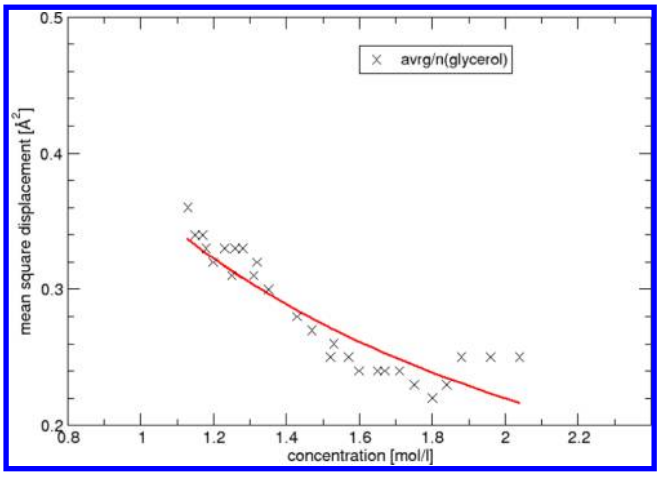

Figure 6. Normalized mean square displacements of all glycerol molecules in the system calculated with Amber10 Ptraj. For each concentration investigated, the average mean square displacement ($\langle |r(t) - r(0)|^2 \rangle$) was computed, divided by the number of molecules, and plotted vs time. As expected, glycerol mobility decreases with increasing concentration of glycerol in the sample solution.

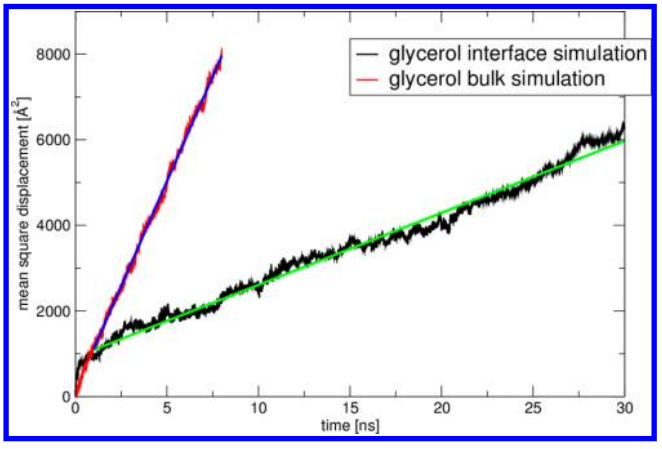

Figure 7. Average mean square displacements, calculated for all atoms of glycerol in the interface simulation (black) and the pure bulk simulation (red), at a glycerol concentration of 1.23 mol L^{-1} (glycerol mole fraction 0.041). Mean square displacements were calculated for the time interval between 3 and 10 ns (7 ns) in the case of the bulk simulation and between 26.2 and 56.2 ns (30 ns) in the case of the interface simulation. Snapshots recorded every ps were used for the analysis. Diffusion coefficient were calculated using $D = (\mathrm{MSD})/(6t)$: $D_{bulk} = 1.63 \times 10^{-5}$ (cm^2)/s; $D_{interface} = 0.28 \times 10^{-5}$ (cm^2)/s.

dx.doi.org/10.1021/la4021355 | *Langmuir* 2013, 29, 11898−11907

glycerol molecules at each concentration. As expected, the mobility of the glycerol molecules decreases with higher concentration.

DISCUSSION

The simulations provide a detailed view of the concentration profiles of the species present in the sample and their molecular interactions in the bulk and at the interface.

The analysis of the distribution of molecules along the *z*-direction of the simulation cell (Figure 3) clearly shows an enrichment of glycerol near the interface, thus ruling out the opposite effect considered as an alternative in the experimental paper.[12] Although the force field used for the simulations may suffer from the approximations inherent in the model, this enrichment of glycerol at the interface is likely to be a real effect. Visual inspection of sample snapshots reveals that the glycerol molecules are frequently oriented with their hydrophobic ends toward the dodecane phase (Figure 8).

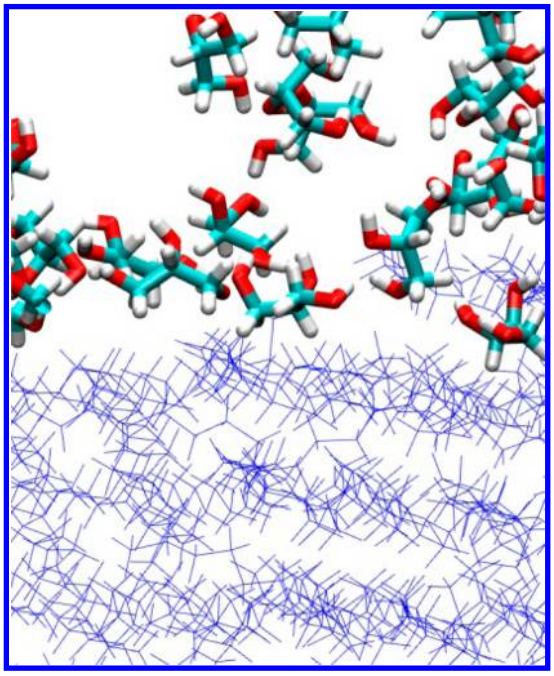

Figure 8. Detailed view of the interface structure from a sample snapshot (50.2 ns, 1.23 mol L^{-1} glycerol in water). CPK sticks, glycerol; blue lines, dodecane. Water molecules are omitted for clarity.

Our finding that there is an accumulation of glycerol near the interface is consistent with the insight gained from previous experimental work, which shows that the local viscosity in the immediate neighborhood of the interface is increased.[12] This observation can be explained by two effects: in the case of a pure water-dodecane interface, the longer lifetime of the MG and BG excited states are due to the specific nature of interfacial water. When glycerol is added to the water phase, the organization of interfacial water is disrupted and in this case the longer excited-state lifetimes can be explained by a larger interfacial concentration of glycerol than in the bulk, consistent with the higher viscosity of concentrated glycerol solutions. Additionally, the presence of the interface can change the potential surface of the dye molecule, as pointed out by Tahara and co-workers.[23]

Furthermore, an enrichment of glycerol near the interface has also been observed experimentally for other types of interfaces formed with glycerol/water mixtures (glycerol/water–air[68] and glycerol/water–lipid interfaces).[69]

The radial distribution functions shown in Figure 9 further support this interpretation. The dye is located at the interface,

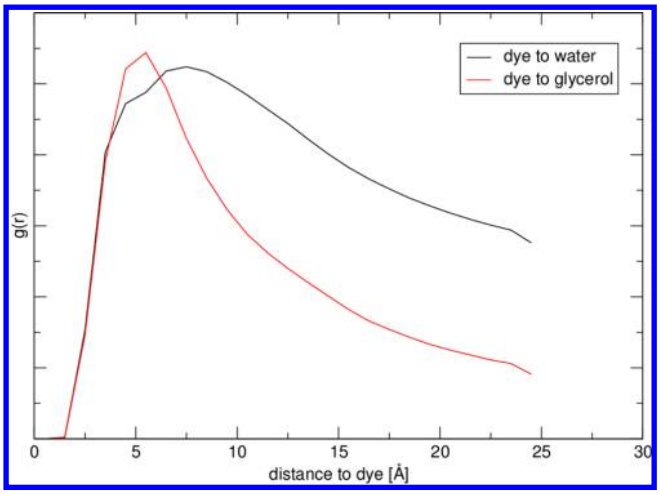

Figure 9. Radial distribution functions calculated for the interaction between the centers of mass of malachite green and glycerol (red), and water (black), respectively. The data shown are for the exemplary system with 1.23 mol L^{-1} glycerol in water (interface simulation).

the radial distribution function calculated for the interaction with glycerol molecules shows a peak at approximately 5 Å from the dye molecule, whereas the water molecules have their maximum approximately 8 Å from the dye. The decrease in the radial distribution functions is enhanced as we have analyzed an interface system. Thus, only one-half-sphere used in the calculation of the radial distribution function is occupied with the glycerol/water mixture, the other half is filled with dodecane.

Our finding that the relative amount of glycerol molecules near the interface decreases with higher concentrations (Figure 4) results from a saturation of glycerol in the first layers near the interface at higher concentrations, and, therefore, more glycerol molecules are found in the bulk. This is consistent with the slower increase of the MG and BG excited-state lifetimes at the interface compared to the bulk water/glycerol mixture with increasing glycerol concentration.

Both dyes (MG and BG), which were initially placed at the interface, remain there (approximately within ±5 Å, Figure 3) for the whole simulation time, in good agreement with experiment.[12] Our observation that the mean deflection of the chromophore axes lies within ±20° from the interface plane (Figure S4 in the Supporting Information) agrees well with the previous measurements by Eisenthal and co-workers.[5] However, we cannot see a clear preference which ring (i.e., phenyl or aniline) protrudes into which phase (alkane or water/glycerol).

While we are confident that the sampling performed in the present study is sufficient to gain insight into the interface structure, it is, however, in principle possible that the SHG signal in the experiment is caused by a minor subpopulation of the adsorbed dye molecules that have a more anisotropic orientation and hence a strong second-order response.

The simulation data also allow us to investigate the dynamics of glycerol molecules in the first and second bulk layers near the interface. In agreement with the analysis shown above (Figure 3), Figure 5 and Figure S1 in the Supporting

dx.doi.org/10.1021/la4021355 | *Langmuir* 2013, 29, 11898–11907

Information show an accumulation of glycerol in two layers next to the interface. The energy cost for a position change of individual glycerol molecules from the first to the second layer decreases more rapidly than the energy barrier that needs to be crossed (Figures S2 and S3 in the Supporting Information). The barrier height (kinetics) does not vary much depending on the glycerol concentration, in contrast to the energy difference between the first and second minima (glycerol layer). The energy gain for a glycerol molecule that hops from the second to the first layer is higher for lower glycerol concentrations, in agreement with the above assumption of a saturation of glycerol near the interface at higher concentrations. Therefore, the diffusional motion of individual glycerol molecules decreases with higher concentration. This agrees well with the analysis of the mean square displacements for the concentration series investigated, shown in the Results section (Figure 6). The influence of the interface on glycerol mobility is further illustrated by the analysis of the average mean square displacements, calculated for glycerol in the interface simulation and in the bulk simulation (Figure 7, glycerol concentration 1.23 mol L^{-1}, glycerol mole fraction 0.041). The diffusion coefficient obtained from this plot for glycerol in the bulk simulation is larger (D_{bulk} = 1.63 × 10^{-5} cm^2 s^{-1}) than that obtained in the interface simulation ($D_{interface}$ = 0.28 × 10^{-5} cm^2 s^{-1}). These values are quite consistent with literature values for glycerol in a dilute solution in water (0.93 × 10^{-5} cm^2 s^{-1}),[61] and for a glycerol/water mixture with a glycerol mole fraction of 0.0432 (0.43 × 10^{-9} m^2 s^{-1}).[62]

Figures S5−S8 in the Supporting Information show the transition dipoles of the dye molecules as obtained from the QM/MM calculations performed on parts of the classical MD simulation trajectories (snapshots were extracted every 100 ps, and the actual time-step was 2 fs). The $S_0 \rightarrow S_2$ transition was analyzed because an 800 nm laser was used in the experiment for the probe pulses. The probe light at 800 nm is two-photon resonant with the $S_0 \rightarrow S_2$ transition of the dyes. A comparison of the transition dipoles that correspond to malachite green molecules fitted on a reference structure obtained from the interface simulation (Figure S6 in the Supporting Information) with those obtained from the bulk simulation (Figure S8 in the Supporting Information) shows that there is no qualitative difference visible between the two cases; that is, the influence (polarization) of the different environments (interface vs bulk) is negligible. The (moderate) variation of the transition dipoles with respect to the molecular frame of the chromophore thus mainly results from the flexibility of the chromophore. This variation must be taken into account in experiments in which the orientation of molecules at the interface is studied. Typically, both the angle between molecular axis and the interface and its distribution are calculated from measured components of the $\chi^{(2)}$ tensor. Nevertheless, the simulations indicate that the angle's distribution calculated this way may be affected by fluctuations of transition dipoles with respect to the molecular frame.

We have observed a similar behavior earlier for tryptophan,[34] where FRET in a flexible system was simulated and we concluded that simulations and the calculation of the actual transition dipoles can make important contributions to understand spectroscopic properties of flexible molecules.

In the interface situation, the transition dipoles (unfitted with respect to the molecular frame of the chromophore) are approximately freely distributed with respect to the interface plane, and most of them show a significant z-component which is visualized in Figure S7 in the Supporting Information for malachite green. In the case of strongly resonant second-harmonic generation, it is this z-component of the transition dipoles that is responsible for the measured signal. The effective contribution of in-plane components averages to zero due to isotropic distribution of transition moments around the z-axis. Therefore, at a given moment in time, a relative contribution of each molecule to the measured second harmonic light depends on the orientation of the probed transition dipole. According to the simulation, this orientation changes on a picosecond time scale, thus it is randomized between consecutive laser pulses, which are a millisecond apart. This means that in a typical experiment, where a large number of pulses (of the order of 1000) is averaged for each data point, there is no defined population and all MG molecules present at the interface contribute equally to the measured signal.

In order to investigate how fast the transition dipoles actually fluctuate (caused by the flexibility of the molecule), we reran a short MD (2000 fs) in which we saved every geometry (every 2 fs) and used these 1000 structures for QM/MM. The results (Figure S9 in the Supporting Information) show that the transition dipoles, in addition to the distribution shown above (100 ps time scale), also show a variation on the fs time scale. The probe laser in the SHG experiment (fwhm 120 fs) would thus perceive only mean orientations of the calculated and plotted (Figure S9 in the Supporting Information) transition dipoles. This, however, does not affect the variation of the transition dipoles on the 100 ps time scale as discussed above (Figures S5−S8 in the Supporting Information).

Our present and previous[34] simulations show that the static pictures frequently used as an approximate description of the position of the transition dipole with respect to the molecular axis needs to be refined with ensembles of transition dipoles which result from intramolecular flexibility, which can be obtained by the simulation approach presented in this work.

■ CONCLUSIONS AND OUTLOOK

Overall, our simulations provide a detailed view of the conclusions and assumptions considering the molecular fine structure of the interface given in the experimental work by Fita, Punzi, and Vauthey.[12] These authors conclude that the increase of viscosity in the interfacial region (compared to the bulk) probably results from a structural modification of water several molecular layers below the interface and that this layer encompasses entirely the aniline groups of either dye, including the alkyl substituents. Our simulations suggest that there is indeed a layer of increased viscosity, but that this is due to an enrichment of glycerol near the interface. Our analyses further support the view that this special layer covers the aniline substituents of the dyes. However, it cannot be ruled out that the influence of the interface on the potential surface of the dye is in part responsible for the slow-down of malachite green or brilliant green excited state deactivation observed in experiment.[23]

The present study shows that molecular simulations can most valuably complement experimental studies, as they allow a direct view on an atomistic scale, which is in many cases inaccessible by experiments. Future studies of the system presented in this work will comprise a detailed analysis of the deactivation mechanism by quantum mechanical/molecular mechanical (QM/MM) methods. Furthermore, nonlinear optical spectroscopic effects like SHG can be explicitly simulated by the quantum mechanical calculation of second

dx.doi.org/10.1021/la4021355 | Langmuir 2013, 29, 11898−11907

order polarizabilities, for a large number of snapshots obtained from the classical MD trajectories presented here. This work is now in progress.

■ ASSOCIATED CONTENT

Supporting Information

Additional figures and tables showing (a) force field parameters not included in the standard gaff parameter files, atom numbering, atom types, and charges for malachite green and brilliant green, (b) concentrations and glycerol particle numbers, (c) potentials of mean force calculated from the distribution functions shown in Figure 5, (d) energy difference between the first glycerol layer and the barrier, (e) energy difference between the first and the second glycerol layer, (f) vectors used for the analysis (Figure S4) of the orientation of the dye chromophores relative to the interface, (g) deflection of the aromatic rings from the *xy*-plane (interface plane) for brilliant green and malachite green, (h) QM/MM results: (S0 → S2) transition dipoles, calculated for the dyes in a point charge environment, fitted and unfitted, interface and bulk simulations, (i) calculated densities and diffusion coefficients of glycerol, glycerol–water mixtures, dodecane, and (j) procedure for interface determination. This material is available free of charge via the Internet at http://pubs.acs.org.

■ AUTHOR INFORMATION

Corresponding Author

*E-mail: Tim.Clark@fau.de.

Notes

The authors declare no competing financial interest.

■ ACKNOWLEDGMENTS

This work was supported by the Deutsche Forschungsgemeinschaft as part of the Excellence Cluster *Engineering of Advanced Materials*. We thank the Regionales Rechenzentrum Erlangen for computing facilities.

■ REFERENCES

(1) Hicks, J. M.; Kemnitz, K.; Eisenthal, K. B.; Heinz, T. F. Studies of liquid surfaces by second harmonic generation. *J. Phys. Chem.* **1986**, *90* (4), 560–562.

(2) Rasing, T.; Shen, Y. R.; Kim, M. W.; Valint, P., Jr.; Bock, J. Orientation of surfactant molecules at a liquid-air interface measured by optical second-harmonic generation. *Phys. Rev. A* **1985**, *31* (1), 537–539.

(3) Zhao, X.; Subrahmanyan, S.; Eisenthal, K. B. Determination of pKa at the air/water interface by second harmonic generation. *Chem. Phys. Lett.* **1990**, *171* (5–6), 558–562.

(4) Castro, A.; Bhattacharyya, K.; Eisenthal, K. B. Energetics of adsorption of neutral and charged molecules at the air/water interface by second harmonic generation: Hydrophobic and solvation effects. *J. Chem. Phys.* **1991**, *95* (2), 1310–1315.

(5) Shi, X.; Borguet, E.; Tarnovsky, A. N.; Eisenthal, K. B. Ultrafast dynamics and structure at aqueous interfaces by second harmonic generation. *Chem. Phys.* **1996**, *205* (1–2), 167–178.

(6) Eisenthal, K. B. Liquid Interfaces Probed by Second-Harmonic and Sum-Frequency Spectroscopy. *Chem. Rev.* **1996**, *96* (4), 1343–1360.

(7) Schneider, L.; Peukert, W. Second Harmonic Generation Spectroscopy as a Method for In Situ and Online Characterization of Particle Surface Properties. *Part. Part. Syst. Charact.* **2006**, *23* (5), 351–359.

(8) Engelhardt, K.; Rumpel, A.; Walter, J.; Dombrowski, J.; Kulozik, U.; Braunschweig, B.; Peukert, W. Protein Adsorption at the Electrified Air–Water Interface: Implications on Foam Stability. *Langmuir* **2012**, *28* (20), 7780–7787.

(9) Rumpel, A.; Novak, M.; Walter, J.; Braunschweig, B.; Halik, M.; Peukert, W. Tuning the Molecular Order of C60 Functionalized Phosphonic Acid Monolayers. *Langmuir* **2011**, *27* (24), 15016–15023.

(10) Schürer, B.; Hoffmann, M.; Wunderlich, S.; Harnau, L.; Peschel, U.; Ballauff, M.; Peukert, W. Second Harmonic Light Scattering from Spherical Polyelectrolyte Brushes. *J. Phys. Chem. C* **2011**, *115* (37), 18302–18309.

(11) Tomalino, L. M.; Voronov, A.; Kohut, A.; Peukert, W. Study of Amphiphilic Polyester Micelles by Hyper-Rayleigh Scattering: Invertibility and Phase Transfer. *J. Phys. Chem. B* **2008**, *112* (20), 6338–6343.

(12) Fita, P.; Punzi, A.; Vauthey, E. Local Viscosity of Binary Water +Glycerol Mixtures at Liquid/Liquid Interfaces Probed by Time-Resolved Surface Second Harmonic Generation. *J. Phys. Chem. C* **2009**, *113* (48), 20705–20712.

(13) Matsuzaki, K.; Nihonyanagi, S.; Yamaguchi, S.; Nagata, T.; Tahara, T. Vibrational Sum Frequency Generation by the Quadrupolar Mechanism at the Nonpolar Benzene/Air Interface. *J. Phys. Chem. Lett.* **2013**, *4* (10), 1654–1658.

(14) Kundu, A.; Watanabe, H.; Yamaguchi, S.; Tahara, T. Agreement between Experimentally and Theoretically Estimated Orientational Distributions of Solutes at the Air/Water Interface. *J. Phys. Chem. C* **2013**, *117* (17), 8887–8891.

(15) Yamaguchi, S.; Kundu, A.; Sen, P.; Tahara, T. Communication: Quantitative estimate of the water surface pH using heterodyne-detected electronic sum frequency generation. *J. Chem. Phys.* **2012**, *137* (15), 151101.

(16) Singh, P. C.; Nihonyanagi, S.; Yamaguchi, S.; Tahara, T. Ultrafast vibrational dynamics of water at a charged interface revealed by two-dimensional heterodyne-detected vibrational sum frequency generation. *J. Chem. Phys.* **2012**, *137* (9), 094706.

(17) Mondal, J. A.; Nihonyanagi, S.; Yamaguchi, S.; Tahara, T. Three Distinct Water Structures at a Zwitterionic Lipid/Water Interface Revealed by Heterodyne-Detected Vibrational Sum Frequency Generation. *J. Am. Chem. Soc.* **2012**, *134* (18), 7842–7850.

(18) Yamaguchi, S.; Watanabe, H.; Mondal, S. K.; Kundu, A.; Tahara, T. "Up" versus "down" alignment and hydration structures of solutes at the air/water interface revealed by heterodyne-detected electronic sum frequency generation with classical molecular dynamics simulation. *J. Chem. Phys.* **2011**, *135* (19), 194705.

(19) Yamaguchi, S.; Shiratori, K.; Morita, A.; Tahara, T. Electric quadrupole contribution to the nonresonant background of sum frequency generation at air/liquid interfaces. *J. Chem. Phys.* **2011**, *134* (18), 184705.

(20) Yamaguchi, S.; Bhattacharyya, K.; Tahara, T. Acid–Base Equilibrium at an Aqueous Interface: pH Spectrometry by Heterodyne-Detected Electronic Sum Frequency Generation. *J. Phys. Chem. C* **2011**, *115* (10), 4168–4173.

(21) Nihonyanagi, S.; Ishiyama, T.; Lee, T.-k.; Yamaguchi, S.; Bonn, M.; Morita, A.; Tahara, T. Unified Molecular View of the Air/Water Interface Based on Experimental and Theoretical $\chi(2)$ Spectra of an Isotopically Diluted Water Surface. *J. Am. Chem. Soc.* **2011**, *133* (42), 16875–16880.

(22) Mondal, S. K.; Yamaguchi, S.; Tahara, T. Molecules at the Air/Water Interface Experience a More Inhomogeneous Solvation Environment than in Bulk Solvents: A Quantitative Band Shape Analysis of Interfacial Electronic Spectra Obtained by HD-ESFG. *J. Phys. Chem. C* **2011**, *115* (7), 3083–3089.

(23) Sen, P.; Yamaguchi, S.; Tahara, T. Ultrafast dynamics of malachite green at the air/water interface studied by femtosecond time-resolved electronic sum frequency generation (TR-ESFG): an indicator for local viscosity. *Faraday Discuss.* **2010**, *145*, 411–428.

(24) Fedoseeva, M.; Richert, S.; Vauthey, E. Excited-State Dynamics of Organic Dyes at Liquid/Liquid Interfaces. *Langmuir* **2012**, *28* (31), 11291–11301.

(25) Richert, S.; Fedoseeva, M.; Vauthey, E. Ultrafast Photoinduced Dynamics at Air/Liquid and Liquid/Liquid Interfaces. *J. Phys. Chem. Lett.* **2012**, *3* (12), 1635−1642.
(26) Wang, H.; Troxler, T.; Yeh, A.-G.; Dai, H.-L. In Situ, Nonlinear Optical Probe of Surfactant Adsorption on the Surface of Micro-particles in Colloids. *Langmuir* **2000**, *16* (6), 2475−2481.
(27) Wang, H.; Yan, E. C. Y.; Borguet, E.; Eisenthal, K. B. Second harmonic generation from the surface of centrosymmetric particles in bulk solution. *Chem. Phys. Lett.* **1996**, *259* (1−2), 15−20.
(28) Adamenko, I. I.; Bulavin, L. A.; Ilyin, V.; Zelinsky, S. A.; Moroz, K. O. Anomalous behavior of glycerol−water solutions. *J. Mol. Liq.* **2006**, *127* (1−3), 90−92.
(29) Chen, C.; Li, W. Z.; Song, Y. C.; Yang, J. A molecular dynamics study of cryoprotective agent − Water−sodium chloride ternary solutions. *J. Mol. Struct.: THEOCHEM* **2009**, *916* (1−3), 37−46.
(30) Li, D.-X.; Liu, B.-L.; Liu, Y.-s.; Chen, C.-l. Predict the glass transition temperature of glycerol−water binary cryoprotectant by molecular dynamic simulation. *Cryobiology* **2008**, *56* (2), 114−119.
(31) Dashnau, J. L.; Nucci, N. V.; Sharp, K. A.; Vanderkooi, J. M. Hydrogen Bonding and the Cryoprotective Properties of Glycerol/Water Mixtures. *J. Phys. Chem. B* **2006**, *110* (27), 13670−13677.
(32) Sundström, V.; Gillbro, T.; Bergström, H. Picosecond kinetics of radiationless relaxations of triphenyl methane dyes. Evidence for a rapid excited-state equilibrium between states of differing geometry. *Chem. Phys.* **1982**, *73* (3), 439−458.
(33) Saikan, S.; Sei, J. Investigation of the conformational change in triphenylmethane dyes via polarization spectroscopy. *J. Chem. Phys.* **1983**, *79* (9), 4154−4158.
(34) Beierlein, F. R.; Othersen, O. G.; Lanig, H.; Schneider, S.; Clark, T. Simulating FRET from Tryptophan: Is the Rotamer Model Correct? *J. Am. Chem. Soc.* **2006**, *128* (15), 5142−5152.
(35) Jäger, C. M.; Hirsch, A.; Schade, B.; Ludwig, K.; Böttcher, C.; Clark, T. Self-Assembly of Structurally Persistent Micelles Is Controlled by Specific-Ion Effects and Hydrophobic Guests. *Langmuir* **2009**, *26* (13), 10460−10466.
(36) Case, D. A.; Darden, T. A.; Cheatham, T. E., III; Simmerling, C. L.; Wang, J.; Duke, R. E.; Luo, R.; Crowley, M.; C.Walker, R.; Zhang, W.; Merz, K. M.; B..Wang; Hayik, S.; Roitberg, A.; Seabra, G.; ; Kolossváry, I.; F.Wong, K.; Paesani, F.; Vanicek, J.; Wu, X.; Brozell, S. R.; Steinbrecher, T.; Gohlke, H.; Yang, L.; Tan, C.; Mongan, J.; Hornak, V.; Cui, G.; Mathews, D. H.; Seetin, M. G.; Sagui, C.; Babin, V.; Kollman, P. A. *AMBER 10*; University of California: San Francisco, 2008.
(37) *Materials Studio 4.4*; Accelrys Inc.: San Diego, CA, 2008.
(38) Dewar, M. J. S.; Zoebisch, E. G.; Healy, E. F.; Stewart, J. J. P. AM1: A New General Purpose Quantum Mechanical Molecular Model. *J. Am. Chem. Soc.* **1985**, *107*, 3902−3909.
(39) Clark, T.; Alex, A.; Beck, B.; Burkhardt, F.; Chandrasekhar, J.; Gedeck, P.; Horn, A.; Hutter, M.; Martin, B.; Rauhut, G.; Sauer, W.; Schindler, T.; Steinke, T. *Vamp 10.0*; Computer-Chemie-Centrum, Universität Erlangen-Nürnberg: Erlangen, Germany, 2003.
(40) Jakalian, A.; Bush, B. L.; Jack, D. B.; Bayly, C. I. Fast, efficient generation of high-quality atomic charges. AM1-BCC model: I. Method. *J. Comput. Chem.* **2000**, *21*, 132−146.
(41) Jakalian, A.; Jack, D. B.; Bayly, C. I. Fast, efficient generation of high-quality atomic charges. AM1-BCC model: II. Parameterization and Validation. *J. Comput. Chem.* **2002**, *23*, 1623−1641.
(42) Wang, J.; Wang, W.; Kollman, P. A.; Case, D. A. Automatic atom type and bond type perception in molecular mechanical calculations. *J. Mol. Graphics Modell.* **2006**, *25*, 247−260.
(43) Jorgensen, W. L.; Chandrasekhar, J.; Madura, J. D.; Impey, R. W.; Klein, M. L. Comparison of simple potential functions for simulating liquid water. *J. Chem. Phys.* **1983**, *79* (2), 926−935.
(44) Perl website, http://www.perl.org/.
(45) Wang, J.; Wolf, R. M.; Caldwell, J. W.; Kollman, P. A.; Case, D. A. Development and Testing of a General Amber Force Field. *J. Comput. Chem.* **2004**, *25*, 1157−1174.
(46) Minofar, B.; Jungwirth, P.; Das, M. R.; Kunz, W.; Mahiuddin, S. Propensity of Formate, Acetate, Benzoate, and Phenolate for the Aqueous Solution/Vapor Interface: Surface Tension Measurements and Molecular Dynamics Simulations. *J. Phys. Chem. C* **2007**, *111* (23), 8242−8247.
(47) Picalek, J.; Minofar, B.; Kolafa, J.; Jungwirth, P. Aqueous solutions of ionic liquids: study of the solution/vapor interface using molecular dynamics simulations. *Phys. Chem. Chem. Phys.* **2008**, *10* (37), 5765−5775.
(48) Ryckaert, J.-P.; Ciccotti, G.; Berendsen, H. J. C. Numerical integration of the cartesian equations of motion of a system with constraints: molecular dynamics of n-alkanes. *J. Comput. Phys.* **1977**, *23* (3), 327−341.
(49) Darden, T.; York, D.; Pedersen, L. Particle mesh Ewald: An N log(N) method for Ewald sums in large systems. *J. Chem. Phys.* **1993**, *98*, 10089−10092.
(50) Essmann, U.; Perera, L.; Berkowitz, M. L.; Darden, T.; Lee, H.; Pedersen, L. G. A smooth particle mesh Ewald method. *J. Chem. Phys.* **1995**, *103*, 8577−8593.
(51) Clark, T.; Alex, A.; Beck, B.; Gedeck, P.; Lanig, H. A Semiempirical QM/MM Implementation and its Application to the Absorption of Organic Molecules in Zeolites. *J. Mol. Model.* **1999**, *5*, 1−7.
(52) Rauhut, G.; Clark, T.; Steinke, T. A Numerical Self-Consistent Reaction Field (SCRF) Model for Ground and Excited States in NDDO-Based Methods. *J. Am. Chem. Soc.* **1993**, *115*, 9174−9181.
(53) Gedeck, P.; Schneider, S. *J. Photochem. Photobiol., A* **1997**, *105*, 165−181.
(54) Schürer, G.; Horn, A. H. C.; Gedeck, P.; Clark, T. *J. Phys. Chem. B* **2002**, *106*, 8815−8830.
(55) Beierlein, F.; Lanig, H.; Schürer, G.; Horn, A. H. C.; Clark, T. Quantum Mechanical/Molecular Mechanical (QM/MM) Docking: An Evaluation for Known Test Systems. *Mol. Phys.* **2003**, *101*, 2469−2480.
(56) Schürer, G.; Lanig, H.; Clark, T. The Mode of Action of Phospholipase A2: Semiempirical MO Calculations Including the Protein Environment. *J. Phys. Chem. B* **2000**, *104*, 1349−1361.
(57) Schürer, G.; Lanig, H.; Clark, T. *Biochemistry* **2004**, *43*, 5414−5427.
(58) Clark, T.; Chandrasekhar, J. NDDO-based CI methods for the prediction of electronic spectra and sum-over-states molecular hyperpolarization. *Isr. J. Chem.* **1993**, *33*, 435−448.
(59) *Jmol 9.1*: an open-source Java viewer for chemical structures in 3D; http://www.jmol.org/ (accessed Jun 22, 2004).
(60) Williams, T.; Kelley, C. *Gnuplot 4.4.3*: an interactive plotting program; http://gnuplot.info (2011).
(61) Hayduk, W.; Laudie, H. Prediction of diffusion coefficients for nonelectrolytes in dilute aqueous solutions. *AIChE J.* **1974**, *20* (3), 611−615.
(62) D'Errico, G.; Ortona, O.; Capuano, F.; Vitagliano, V. Diffusion Coefficients for the Binary System Glycerol + Water at 25 °C. A Velocity Correlation Study. *J. Chem. Eng. Data* **2004**, *49* (6), 1665−1670.
(63) Christoph, R.; Schmidt, B.; Steinberner, U.; Dilla, W.; Karinen, R. Glycerol. In *Ullmann's Encyclopedia of Industrial Chemistry, Electronic Release*; Wiley-VCH Verlag GmbH & Co. KGaA: Weinheim, 2012; Vol. *17*, pp 77−81.
(64) Aylward, G. H.; Findlay, T. J. V. *Datensammlung Chemie in SI Einheiten*, 2nd ed.; Verlag Chemie: Weinheim, 1986.
(65) Humphrey, W.; Dalke, A.; Schulten, K. VMD - Visual Molecular Dynamics. *J. Mol. Graphics* **1996**, *14*, 33−38.
(66) VMD web page; http://www.ks.uiuc.edu/Research/vmd/; accessed Mar 30, 2012.
(67) Loeffler, H. Handy Routines for Ptraj/Cpptraj. Science and Technology Facilities Council Daresbury Laboratory web page; http://www.stfc.ac.uk/cse/25249.aspx; accessed Aug 1, 2013.
(68) Baldelli, S.; Schnitzer, C.; Shultz, M. J.; Campbell, D. J. Sum Frequency Generation Investigation of Glycerol/Water Surfaces. *J. Phys. Chem. B* **1997**, *101* (23), 4607−4612.
(69) Pocivavsek, L.; Gavrilov, K.; Cao, K. D.; Chi, E. Y.; Li, D.; Lin, B.; Meron, M.; Majewski, J.; Lee, K. Y. C. Glycerol-Induced

Membrane Stiffening: The Role of Viscous Fluid Adlayers. *Biophys. J.* **2011**, *101* (1), 118−127.